A least-squares method for multisurface unfolding

MICHEL LÉGER and MURIEL THIBAUT*

Institut Français du Pétrole, Direction de Recherche Géophysique-Instrumentation, BP 311, 92506
Rueil-Malmaison, France

JEAN-PIERRE GRATIER

L.G.I.T.-C.N.R.S., Observatoire de Grenoble, Université Joseph Fourier, I.R.I.G.M., BP 53X, 38041
Grenoble, France

and

JEAN-MARIE MORVAN

Université Claude Bernard Lyon I, Institut de Mathématique et d'Informatique, Bâtiment 101, 43
boulevard du 11 Novembre, 69622 Villeurbanne, France

Abstract—Geologic structures are mostly known from scattered data, and structures such as folds or faults are drawn in between by using interpolation, which is often based on geologically poor assumptions, such as smoothness. The need for more accuracy leads to restoration techniques in which more realistic assumptions are introduced. In this context, we have tested a multisurface unfolding procedure. We use a least-squares formulation involving the following criteria: initial horizontality, bed-length conservation (during slip on bedding) and local volume conservation. Weighted optimization of these criteria gives a compromise between them if they are conflicting. We have succesfully tested the method on various theoretical examples and on an analog model: the 'paperback experiment'. © 1997 Elsevier Science Ltd.

INTRODUCTION

Large geologic structures are mostly known from scattered data, and interpolation is often needed among these data in order to draw structures such as folds or faults. For example, when a set of isolated or fuzzy data (outcrops, structures in boreholes, seismic reflectors) yields, from place to place, the location of folded layers, there are always many possibilities for drawing these layers. Firstly, each piece of data does not have the same reliability. For example, the geometry and the location of a given layer may be more reliable with outcrops than with seismic data. So it is important to be able to express our confidence in the data. Secondly, since folded and faulted structures are deformed, assumptions as to the geometry and kinematics of deformation are always required to choose the interpolation method. For example, assuming volume and bed-length (hence area) conservation and kinematic boundary conditions (décollement surface, displacement), the construction of balanced cross-sections can be used to develop a reasonable structural interpretation of folded and faulted structures (Dahlstrom, 1969; Suppe, 1983; Woodward *et al.*, 1985). However, such balanced cross-section construction methods are limited to two dimensions with a plane strain assumption. When dealing with arcuate folds and fault zones, the plane strain assumption is not necessarily realistic (Ramsay, 1969; Ramsay and Huber, 1987). Assuming simple fault and fold kinematics, for example, if all the slip vectors for the faults (Barr, 1985) or the flexural-slip (McCoss, 1988) have parallel map projections, direct three-dimensional restoration is possible. However, in this case the simplicity of the kinematics limits the application of the methods. From a general point of view, for such three-dimensional problems, there are at least two types of assumptions for the mechanical behaviour of the folded surfaces: simple shear folding or flexural-slip folding.

Simple shear was assumed by Gibbs (1983) and Kerr *et al.* (1993) (heterogeneous simple shear with constant shear direction) and by Shaw *et al.* (1994) (fault-bend folds with variable amount, constant direction displacement). The automatic method developed by Kerr *et al.* (1993) enables them to determine the three-dimensional normal fault geometry from the geometry of deformed hanging wall horizons, and thus to balance the structure when both faults and folds are approximately known. The technique proposed by Shaw *et al.* (1994) (axial mapping surface) led to a better understanding of natural three-dimensional structures. In both cases, the (strong) simple shear assumption must be confirmed in the field, for example by observation of distortion within the layering (Fig. 1a).

*Present address: 4 rue Auguste Simon, 94700 Maisons-Alfort, France.

Another possibility is to assume flexural-slip folds (Ramsay, 1967) with no distortion within the curved surface (Fig. 1b). A finite element method (UNFOLD program) based on this assumption has been developed by Gratier et al. (1991). This program can be used to test the geometry of flexural-slip folds by trial and error, and, by comparing deformed and restored folded and faulted structures, to establish a plausible total finite displacement field associated with this deformation (Gratier and Guillier, 1993). From a geometric point of view, Gaussian curvature (equal to the product of the two principal curvatures) remains invariant under isometric bending, i.e. constant bed-length buckling. If layers are flat at deposition, Gaussian curvature remains close to zero after folding. Several authors such as Bennis et al. (1991), Lisle (1992) and Léger et al. (1995) have used this criterion to distinguish between developable and non-developable surfaces. A surface unfolding program (PATCHWORK), based on the algorithm of Bennis et al. (1991), has been developed at the Institut Franais du Pétrole, and is used to test the developability of a single layer. The main limitation of these two programs is that they have to treat each layer successively and independently. Thus, we thought it would be interesting to develop a multisurface unfolding method that is able to treat layered blocks (bounded by faults or arbitrary surfaces) as a whole.

The choice of one of the two basic assumptions (simple shear or flexural-slip) must be made by observation of deformation markers: distortion (Fig. 1a) or rigid rotation (Fig. 1b) within the layers. Simple shear leading to similar folds is presumed to occur in metamorphic rocks (Ramsay, 1967). However, this type of deformation may also develop in incompetent hanging wall sedimentary horizons, for example above a normal fault associated with both compaction and extension (Kerr et al., 1993). Flexural-slip is typically the mechanism of folding under shallow crustal conditions (within the first 5–6 km depth for competent layers such as limestones or sandstones, Ramsay and Huber, 1987).

Under the flexural-slip assumption, we use an inver-

Fig. 2. Unfolding viewed as the transformation Ψ of a folded foliation $\tilde{\mathcal{F}}$ into an unfolded foliation $\mathcal{F}$. The leaves of $\mathcal{F}$ should be horizontal. Ψ transforms 'binding surface' $\tilde{B}$ (where leaves cannot slip on each other) to B. The binding is shaded.

sion method involving three least-squares criteria: initial horizontality, bed-length conservation and volume conservation (Thibaut, 1994). Only one scale of folding is considered (second-order folds are neglected). In the paper we will use the word *foliation* in its *geometrical* sense. Geometrically, a foliation $\mathcal{F}$ is an infinite set of continuous and non intersecting surfaces, called leaves, stacked together so as to fill some volume V (mathematical definition of foliations is given in Léger et al., 1995). Each point of foliated volume V belongs to one and only one leaf of $\mathcal{F}$. For the sake of simplicity we identify a foliated domain $(V, \mathcal{F})$ and foliation $\mathcal{F}$ in what follows. Using the geometrical concept of foliation as a tool, we define the unfolding process as the transformation Ψ that maps a known folded, deformed foliation, $\tilde{\mathcal{F}}$, into an unknown, horizontally restored foliation $\mathcal{F}$ (Fig. 2). Throughout this paper, '~' refers to the folded state and '⁻' to the restored state.

AN INVERSION APPROACH TO FOLIATION UNFOLDING

The inverse problem approach

To unfold a regular curve isometrically into a straight line is always possible. However, to unfold a regular surface isometrically into a piece of a plane is possible only for very particular surfaces, called developable surfaces, which may be cylinders, cones or more general surfaces generated by the tangent to some curve in space. The Gaussian curvature of these surfaces is everywhere zero.

Since geologic surfaces are seldom *strictly* developable, the bed-length conservation hypothesis cannot be *exactly* met in consistency with initial flatness. For this reason, we need an unfolding method that uses this hypothesis in a flexible way, for instance in a least-squares sense (Etchecopar, 1977; Cobbold and Percevault, 1983). Therefore, we have chosen the inverse problem approach, i.e. multicriteria optimization, because it can give an unfolded foliation such that the various hypotheses needed can all be met *at best*. Except for the 'known
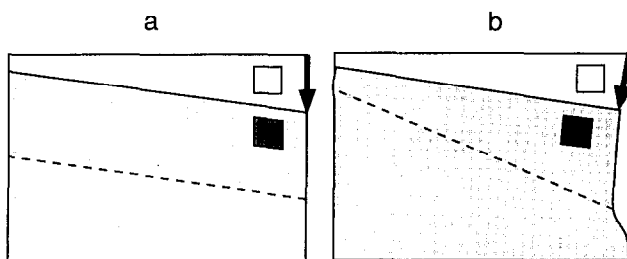

Fig. 1. Map view of two types of models for deformation associated with folding. (a) Simple shear folding with constant direction of shearing (arrow). (b) Flexural-slip folding with rigid rotation of the back limb (arrow) and no bed-length change. The dotted lines are the projections of the axial surface of the folds. Open squares are undeformed markers, shaded squares are the deformed ones in the back limb.
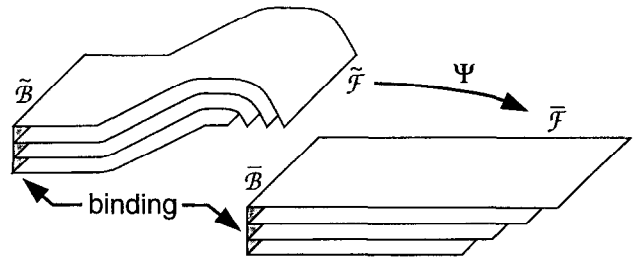
binding condition', our approach consists of defining one objective function per hypothesis and in minimizing their weighted sum. The greater our confidence in a hypothesis, the higher will be the corresponding weight. Each objective function measures to what extent the hypothesis is not met, so that the minimization of the overall objective function will give the best possible compromise consistent with the levels of confidence in the various hypotheses.

Commonly, physics is concerned with predicting the effect of a known excitation on a known system, whereas geophysics attempts to recover Earth properties from the measured effect and given excitation. For this reason, inversion techniques are widely used by geophysicists. In general terms, inversion consists of two main steps, the *forward problem* and the *inverse problem*. The forward problem, $\mathbf{d} = f(\mathbf{p})$, gives computed data vector $\mathbf{d}$, as a map of unknown parameter vector $\mathbf{p}$, which requires an assumption, i.e. an initial guess $\mathbf{p}_0$ of $\mathbf{p}$. The inverse problem consists in optimizing $\mathbf{p}$ so as to minimize the objective function $Q(\mathbf{p}) = \|\mathbf{f}(\mathbf{p}) - \mathbf{d}_0\|^2$, which measures the discrepancy between computed data $\mathbf{d}$ and observed data $\mathbf{d}_0$, $\| \cdot \|$ denoting a norm in the data vector space (Tarantola, 1987). For instance, the seismic wave velocity field in the Earth is usually determined via travel-time inversion.

Now we will describe in detail the geological data that we will use to restore a folded foliation in its initial undeformed state.

Geometric formulation of the unfolding process

We define the unfolding process in geometric terms as the mapping Ψ that minimizes the overall objective function

$$Q(\Psi) = w_h Q_h(\Psi) + w_l Q_l(\Psi) + w_v Q_v(\Psi) \qquad (1)$$

where w_* is the weight of objective function Q_*, with $*$ being h for the horizontality criterion, l for bed-length conservation or v for volume conservation. Since $Q(\Psi)$ is left unchanged by pure sliding of the leaves over each other, it is necessary to constrain Ψ so as to prevent this indeterminacy. In two-dimensional section balancing, this constraint is provided by a pin-line. For multisurface unfolding, we assume that the surfaces are linked by a binding, as at the back of a book (Fig. 2). Let $\tilde{B}$ and $\bar{B}$ be the binding surfaces, in the folded and unfolded states, respectively, so that

$$\Psi(\tilde{B}) = \bar{B}. \qquad (2)$$

In practice, we will usually assume that $\bar{B} = \tilde{B}$ meaning that the binding does not itself deform.

Horizontality. To unfold a foliation, we constrain the unit vector $\bar{e}_3(\bar{m})$, normal to the leaves of the unfolded foliation $\bar{\mathcal{F}}$ at any point $\bar{m}$, to be as nearly vertical as possible (Fig. 3). Consequently, we unfold the foliation $\bar{\mathcal{F}}$
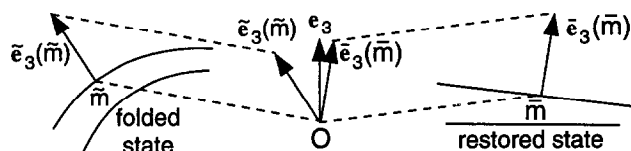

Fig. 3. Unit vector $\tilde{e}_3(\tilde{m})$ is normal to the leaves of folded foliation $\tilde{\mathcal{F}}$, and unit vector $\bar{e}_3(\bar{m})$ is normal to the leaves of restored foliation $\bar{\mathcal{F}}$. Unit vector e_3 denotes the upward vertical. Unit vectors $\tilde{e}_3(\tilde{m})$ or $\bar{e}_3(\bar{m})$, which are drawn based at points $\bar{m}$ or $\tilde{m}$ on the leaf, may be viewed as a mapping, known as the Gauss mapping, from points $\tilde{m}$ or $\bar{m}$ to points $\tilde{e}(\tilde{m})$ or $\bar{e}(\bar{m})$ of the unit sphere centred at the origin O.

by constraining foliation $\bar{\mathcal{F}} = (\Psi)(\tilde{\mathcal{F}})$ to minimize the objective function

$$Q_h(\Psi) = \frac{1}{2} \int_{\tilde{\mathcal{F}}} \|\bar{e}_3(\Psi(\tilde{m})) - e_3\|^2 d\tilde{m} \qquad (3)$$

where e_3 is the upward vertical unit vector. In this equation, the squared verticality misfit $\|\bar{e}_3 - e_3\|^2$ is computed at point $\bar{m} = \Psi(\tilde{m})$, in unknown unfolded foliation $\bar{\mathcal{F}}$, the one that we want to constrain to be horizontal, but is assigned via Ψ to point $\tilde{m}$ in the known folded foliation $\tilde{\mathcal{F}}$ for integration purpose. Note that $\bar{e}_3$ may be viewed as a mapping, the Gauss mapping, from a point $\bar{m}$ in $\bar{\mathcal{F}}$ to a point $\bar{e}_3(\bar{m})$ in the unit sphere centred at the origin.

Bed-length conservation. First, we will define in geometric terms the tangential strain tensor induced by the unfolding process. Then, we will formulate the bed-length conservation hypothesis.

A strain tensor is usually computed by comparing an orthonormal base with its image under a transformation. Formulae are simple where strains and rotations are small. For unfolding, large rotations may occur. Therefore, we use a specific orthonormal base of the tangent plane in the unfolded foliation in order to compute the tangential strain tensor.

Let us consider an orthonormal base $(\tilde{e}_1(\tilde{m}), \tilde{e}_2(\tilde{m}))$ of the tangent plane $T_{\tilde{m}}\tilde{\mathcal{F}}_{\tilde{m}}$ to the leaf $\tilde{\mathcal{F}}_{\tilde{m}}$ at point $\tilde{m}$ of folded foliation $\tilde{\mathcal{F}}$. The first derivative $d\Psi$ of unfolding process Ψ (Ψ transfoms points and $d\Psi$ transforms vectors at a point) maps this base into a base $(d\Psi(\tilde{e}_1), d\Psi(\tilde{e}_2))$ from which we derive an orthonormal base $(\bar{e}_1, \bar{e}_2)$ in the following way (Fig. 4):

$$\begin{cases} \bar{e}_1 = \dfrac{d\Psi(\tilde{e}_1)}{\|d\Psi(\tilde{e}_1)\|} \\[2mm] \bar{e}_2 = \bar{e}_3 \times \bar{e}_1 \\[2mm] \bar{e}_3 = \dfrac{d\Psi(\tilde{e}_1) \times d\Psi(\tilde{e}_2)}{\|d\Psi(\tilde{e}_1) \times d\Psi(\tilde{e}_2)\|}, \end{cases} \qquad (4)$$

with $\|v\|$ denoting the norm of vector v and $\times$ the cross-product. Then we define tangential strain tensor ε_{ij} by

$$\varepsilon_{ij} = \frac{1}{2}(\langle d\Psi(\bar{e}_i), \bar{e}_j \rangle + \langle d\Psi(\bar{e}_j), \bar{e}_i \rangle) - \delta_{ij}, \qquad (5)$$

where $\langle , \rangle$ denotes the dot product and where $\delta_{ij} = 1$ if $i = j$ and $\delta_{ij} = 0$ if $i \neq j$.
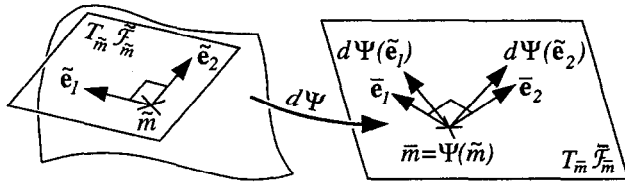
Fig. 4. $(\tilde{e}_1(\tilde{m}), \tilde{e}_2(\tilde{m}))$ is an orthonormal base of plane $T_{\tilde{m}} \tilde{\mathcal{F}}_{\tilde{m}}$ tangent to leaf $\tilde{\mathcal{F}}_{\tilde{m}}$ at $\tilde{m}$. Similarly, $(\bar{e}_1(\bar{m}), \bar{e}_2(\bar{m}))$ is an orthonormal base of plane $T_{\bar{m}} \mathcal{F}_{\bar{m}} = d\Psi(T_{\tilde{m}} \tilde{\mathcal{F}}_{\tilde{m}})$ tangent to leaf $\mathcal{F}_{\bar{m}} = \Psi(\tilde{\mathcal{F}}_{\bar{m}})$ at $\bar{m} = \Psi(\tilde{m})$. We derive the tangential deformation induced by Ψ from the comparison of bases $(d\Psi(\tilde{e}_1), d\Psi(\tilde{e}_2))$ and $(\bar{e}_1, \bar{e}_2)$. Note that we have chosen $\bar{e}_1 = d\Psi(\tilde{e}_1)/ \|d\Psi(\tilde{e}_1)\|$ in the text.

We define tangential strain intensity by

$$e = \frac{1}{2}(\varepsilon_{11}^2 + 2\varepsilon_{12}^2 + \varepsilon_{22}^2) = \frac{1}{2}(\epsilon_1^2 + \epsilon_2^2), \qquad (6)$$

where ϵ_1 and ϵ_2 are the principal strains. This is equivalent to

$$e = \frac{1}{2}[(\|d\Psi(\tilde{e}_1)\| - 1)^2 + (\|d\Psi(\tilde{e}_2)\| - 1)^2 \\ + 2\langle d\Psi(\tilde{e}_1), d\Psi(\tilde{e}_2)\rangle^2] \qquad (7)$$

which is more convenient since the computation of the tangential base $(\bar{e}_1, \bar{e}_2)$ is avoided. Finally, we express the bed-length conservation hypothesis in the following way: tangential strain intensity should everywhere be zero. If this is the case, then unfolding map Ψ is a tangential isometry and the following objective function is zeroed:

$$Q_l = \int_{\tilde{\mathcal{F}}} e(\Psi(\tilde{m})) d\tilde{m}$$

$$= \frac{1}{2} \int_{\tilde{\mathcal{F}}} [(1 - \|d\Psi(\tilde{e}_1)\|)^2 + (1 - \|d\Psi(\tilde{e}_2)\|^2 \qquad (8)$$

$$+ 2\langle d\Psi(\tilde{e}_1), d\Psi(\tilde{e}_2)\rangle^2] d\tilde{m}.$$

Volume conservation. In general, a map Ψ is locally volume conserving if and only if

$$\langle d\Psi(v_1) \times d\Psi(v_2), d\Psi(v_3)\rangle = \langle v_1 \times v_2, v_3\rangle \qquad (9)$$

for any linearly independent vectors v_1, v_2 and v_3 at any point (Fig. 5). In particular, with $(v_1,v_2,v_3) = (\tilde{e}_1,\tilde{e}_2,\tilde{e}_3)$, volume is conserved if the objective function

$$Q_v = \frac{1}{2} \int_{\tilde{\mathcal{F}}} \|1 - \langle d\Psi(\tilde{e}_1) \times d\Psi(\tilde{e}_2), d\Psi(\tilde{e}_3)\rangle\|^2 d\tilde{m} \qquad (10)$$

is zeroed. Since the base $(\tilde{e}_1,\tilde{e}_2,\tilde{e}_3)$ is orthonormal, $\langle \tilde{e}_1 \times \tilde{e}_2,\tilde{e}_3\rangle = 1$ and $\langle d\Psi(\tilde{e}_1) \times d\Psi(\tilde{e}_2), d\Psi(\tilde{e}_3)\rangle$ is the determinant of the Jacobian matrix $d\Psi$.
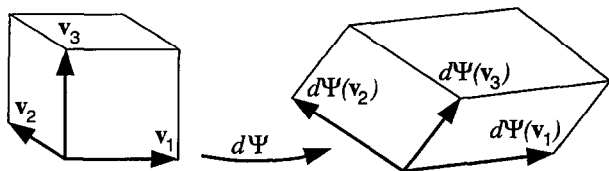

Fig. 5. Volume variation at a point under transformation Ψ, defined as the relative difference between the volume of the parallelepiped spanned by vectors v_1, v_2 and v_3 and the volume of the parallelepiped spanned by vectors $d\Psi(v_1)$, $d\Psi(v_2)$ and $d\Psi(v_3)$.

Of course, by volume conservation, as expressed by $Q_v = 0$, we mean that volume is conserved *everywhere locally.* An *overall* volume conservation, such as expressed by $\int_{\tilde{\mathcal{F}}} d\tilde{m} = \int_{\mathcal{F}} d\bar{m}$ is only relevant in the particular case of incompressible flow (salt diapirs for instance).

The unfolding process in terms of parameterizations

The numerical description and handling of recumbent folds or blocks of any shape are difficult, especially if the boundaries of these blocks are unknown. To cope with these difficulties, we choose to describe foliations via parameterizations (Fig. 6), $\tilde{\mathcal{F}}$ via $\tilde{\Phi}$ and $\mathcal{F}$ via $\bar{\Phi}$. We choose the same curvilinear coordinate domain U for $\tilde{\Phi}$ and $\bar{\Phi}$ to express map Ψ in terms of parameterizations $\tilde{\Phi}$ and $\bar{\Phi}$ (Fig. 7). Hence we have $\Psi(.) = \bar{\Phi}(\tilde{\Phi}^{-1}(.))$ and $d\Psi(.) = d\bar{\Phi}(d\tilde{\Phi}^{-1}(.))$. For both foliations $\tilde{\mathcal{F}}$ and $\mathcal{F}$, we assume that the third curvilinear u^3 is constant on each leaf.

Previous geometric objective functions may be written using parameterizations $\tilde{\Phi}$ and $\bar{\Phi}$. The horizontally objective function becomes
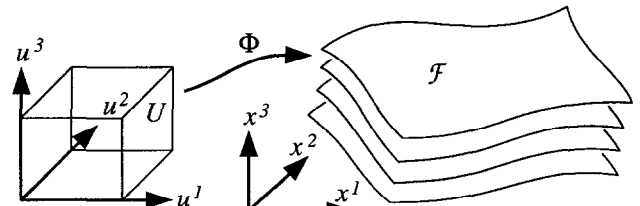

Fig. 6. Parametric representation Φ maps curvilinear coordinates u^1, u^2 and u^3 into Cartesian coordinates x^1, x^2 and x^3 of points in foliation $\mathcal{F}$. All points in a leaf in $\mathcal{F}$ have the same value of coordinate u^3.
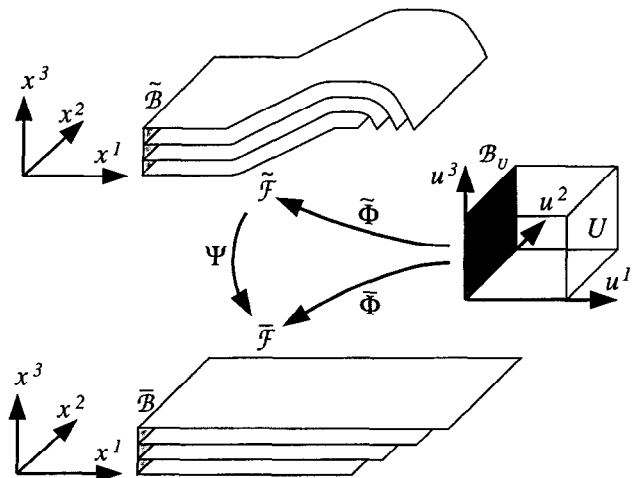

Fig. 7. Unfolding in terms of parameterizations. Folded foliation $\tilde{\mathcal{F}}$ is described by a parameterization $\tilde{\Phi}$ which maps an arbitrary curvilinear coordinate domain U onto $\tilde{\mathcal{F}}$. Similarly, a parameterization $\bar{\Phi}$ maps the same domain U onto unfolded foliation $\mathcal{F}$. The unknown of the problem, which is the unfolding process Ψ in geometrical terms, becomes $\bar{\Phi}(.) = \Psi(\tilde{\Phi}(.))$ in terms of parameterizations. Parameterization $\tilde{\Phi}$ should match the given binding $\tilde{B}$, i.e. $\tilde{\Phi}(\tilde{\Phi}^{-1}(\tilde{B})) = \tilde{B}$, where $\tilde{\Phi}^{-1}(\tilde{B}) = B_U$ implies $\bar{\Phi}(B_U) = \bar{B}$.

$$Q_h(\bar{\Phi}) = \frac{1}{2}\int_U \|\bar{e}_3(\bar{\Phi}(u)) - e_3\|^2 |d\tilde{\Phi}| du, \qquad (13)$$

where $|d\tilde{\Phi}|$ is the determinant of the Jacobian matrix $d\tilde{\Phi}$. This is a simple change of variable from $\tilde{\mathcal{F}}$ to U. Since u^3 is constant on the leaves of $\tilde{\mathcal{F}}$, we may take $\bar{e}_3 = (\bar{\Phi}_{,1} \times \bar{\Phi}_{,2})/\|\bar{\Phi}_{,1} \times \bar{\Phi}_{,2}\|$ and where $\bar{\Phi}_{,1}$ and $\bar{\Phi}_{,2}$ are the first derivatives of $\bar{\Phi}$ with respect to curvilinear coordinates u^1 and u^2. Other objective functions can be written in the same way:

$$Q_l(\bar{\Phi}) = \frac{1}{2}\int_U (1 - \|d\bar{\Phi}(d\tilde{\Phi}^{-1}(\tilde{e}_1))\|)^2$$
$$+ 2\langle d\bar{\Phi}(d\tilde{\Phi}^{-1}(\tilde{e}_1)), d\bar{\Phi}(d\tilde{\Phi}^{-1}(\tilde{e}_2))\rangle^2 \qquad (12)$$
$$+ (1 - \|d\bar{\Phi}(d\tilde{\Phi}^{-1}(\tilde{e}_2))\|)^2]|^2 d\tilde{\Phi}| du$$

for bed-length conservation and

$$Q_v(\bar{\Phi}) = \frac{1}{2}\int_U |1 - \langle d\bar{\Phi}(d\tilde{\Phi}^{-1}(\tilde{e}_1)) \times d\bar{\Phi}(d\tilde{\Phi}^{-1}(\tilde{e}_2)),$$
$$d\bar{\Phi}(d\tilde{\Phi}^{-1}(\tilde{e}_3))\rangle|^2 d\tilde{\Phi}| du \qquad (13)$$

for volume conservation.

Discretization and optimization

We discretize (i.e. we choose a finite dimensional subspace of) the space of the maps $\bar{\Phi}$ and $\tilde{\Phi}$ by using cubic B-spline tensor products. The B-spline coefficients of $\bar{\Phi}$ build unknown parameter vector $\mathbf{p}$ (see section 'The inverse problem approach'). Note that the observed foliation $\tilde{\mathcal{F}}$ is given via fixed map $\tilde{\Phi}$.

Our forward problem f consists in evaluating $\|\bar{e}_3 - e_3\|$ for horizontality, $1 - \|d\Psi(\tilde{e}_1)\|$, $1 - \|d\Psi(\tilde{e}_2)\|$ and $\langle d\Psi(\tilde{e}_1), d\Psi(\tilde{e}_2)\rangle$ for bed-length conservation and $\langle d\Psi(\tilde{e}_1) \times d\Psi(\tilde{e}_2), d\Psi(\tilde{e}_3)\rangle$ for volume conservation, at the nodes of a regular grid in curvilinear coordinates domain U. These quantities build computed data vector $\mathbf{d}$ which should be as close as possible to zero. Hence the 'observed' data vector $\mathbf{d}_0$ is zero.

Our inverse problem consists of minimizing the overall objective function of Eq. (1). To do this, we have chosen the Gauss–Newton procedure, which consists in iteratively solving the linear system $(\mathbf{J'J})\delta\mathbf{p} = -\mathbf{J'}\delta\mathbf{d}$, where $\mathbf{J}$ is the Jacobian matrix of the map $\mathbf{f}$, $\mathbf{J'}$ is its transpose, $\delta\mathbf{p}$ is the B-spline coefficient modification vector computed at each iteration, and $\delta\mathbf{d}$ is the vector of data misfits. Here, $\delta\mathbf{d} = \mathbf{d}$ since $\mathbf{d}_0 = 0$. The equality constraints corresponding to the known binding surface are taken into account by using the technique of Lagrange multipliers.

THEORETICAL EXAMPLES

Now we give the results of our method applied to several theoretical examples.

In order to quantify the quality of the unfolding, we compute several indices that measure how well the various assumptions are met. For each objective function $Q_* = \frac{1}{2}\int_{\tilde{\mathcal{F}}} q_*^2 d\tilde{m}$, we define an index

$$I_* = \sqrt{\frac{\int_{\tilde{\mathcal{F}}} q_*^2 d\tilde{m}}{\int_{\tilde{\mathcal{F}}} d\tilde{m}}} \qquad (14)$$

which represents the RMS (root-mean-square) value of quantity q_*. The horizontality index I_h is the RMS value of

$$q_h = \|\bar{e}_3 - e_3\| \qquad (15)$$

which represents, if $\bar{e}_3 \approx e_3$, the angle between the normal $\bar{e}_3$ to the leaf and the vertical direction e_3 (Eq. 3). We give this angle in degrees in the following. The bed-length conservation index I_l is the RMS value of

$$q_l = \sqrt{2e} = \sqrt{\epsilon_1^2 + \epsilon_2^2}, \qquad (16)$$

where ϵ_1 and ϵ_2 are the eigenvalues of the tangential strain tensor ε_{ij} (see Eqs 5–8). Lastly, the volume index I_v is the RMS value of relative volume variation

$$q_v = |\langle d\Psi(\tilde{e}_1) \times d\Psi(\tilde{e}_2), d\Psi(\tilde{e}_3)\rangle - 1| \qquad (17)$$

(Eq. 10). These three indices are computed over the whole foliation.

Figure 8 shows a cross-section of a cylindrical thrust used for all theoretical examples. Figure 9 represents the initial guess for the unfolded foliation. This initial guess corresponds to the parameter space U, so that $\bar{\Phi}$ is initially trivial. The binding is always displayed on the left-hand side. Binding and ramp both strike north–south. These models involve 1200 B-spline parameters: 20 parameters in u^1 (with $u^1 = 0$ on the binding), 5 parameters in u^2 and 4 parameters in u^3 for the 3 Cartesian coordinates x, y, z. Note that, even at the discrete step, a foliation involves an infinite number of leaves, although 4 parameters in u^3 here means only 4 independent surfaces in that foliation. The rest are interpolated by the B-splines. The known position of the binding involves 60 equality constraints.
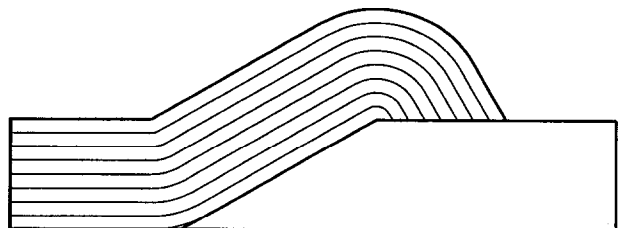

Fig. 8. Cross-section of the folded foliation $\mathcal{F}$ studied in the theoretical examples. The ramp dips at 30° and the bedding dips at 60° in front of the thrust. This structure is almost balanced since the theoretical dip of the ramp below the restored thrust is 31.6°.
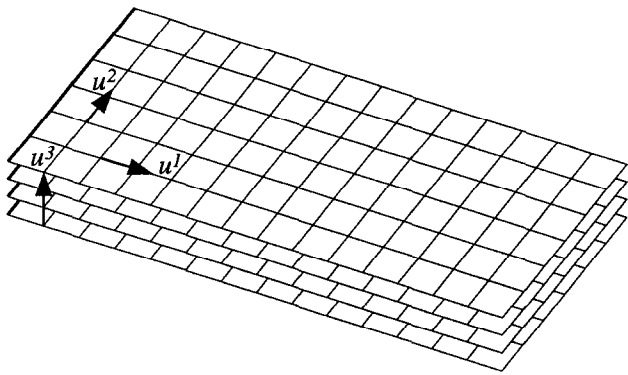
Fig. 9. The initial guess for the unfolded foliation used for all the theoretical examples. For all following figures, the lines drawn on the foliation leaves are iso-u^1 and iso-u^2 contours, u^1 and u^2 being the curvilinear coordinates. The left side of the foliation, in thick lines, is the binding.

A thick thrust

Figure 10(a) shows a thick folded cylindrical thrust and Fig. 10(b) shows the result of the unfolding process. Table 1 shows that bed-length and volume are very well conserved by the unfolding process, whereas horizontality is achieved to within about 5°. We have computed dip values at 50 points spread out on the ramp of the thrust. The average orientation is 000/40W and the standard deviation is 13°, whereas the exact orientation is 000/31.6W. Figure 10(b) shows that numerical errors are concentrated at the bottom of the ramp since dip is clearly steeper there (arrow).

This model required a large number of iterations to converge because of the two singular lines, where the fold is a *chevron*. These singular lines are visible at the bottom of the ramp for the top leaf and at the top of the ramp for the bottom leaf. Since we use twice differentiable B-splines, this cannot be achieved without zeroing the Jacobian of the parameterization. This induces numerical problems because meshes are tiny in the vicinity of these lines. Therefore, several parameters have slight effects on the objective functions. Consequently, they are very poorly determined by the optimization. Indeed, Fig. 10(b) suggests that horizontality is generally to within 5°, except in the vicinity of these lines, where it is worse.
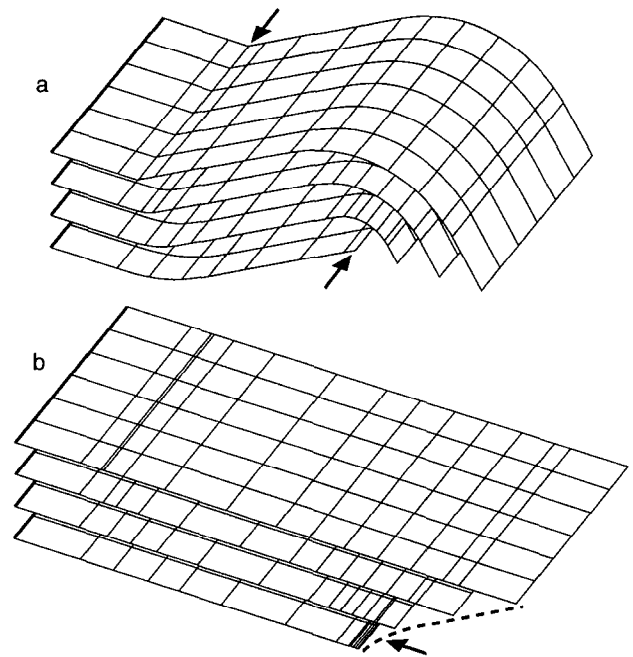

Fig. 10. A thick thrust. (a) Folded structure $\tilde{\mathcal{F}}$. Arrows denote singular lines along which the fold is a *chevron*. (b) Unfolded structure $\mathcal{F}$. Arrow denotes steeper dips below the ramp.

A crooked parameterization

Figure 11 shows a cylindrical foliation with vertical front and rear faces. Our purpose is to show that, due to our geometric formulation of the unfolding process, the crookedness of the parameterization chosen to represent the foliation will not perturb the verticality of the front and rear faces, which assesses the quality of the method. Foliation in Fig. 11 is the same as in Fig. 10(a), but the thickness has been reduced by 15% at top and bottom. The two singular lines and their problematic vicinity are now absent, and the accuracy of the numerical computations is thus improved. The top view of the result (Fig. 12b) clearly demonstrates the validity of this approach, since the two faces remain, as expected, vertical and perpendicular to the binding. Quality indices shown in Table 1 are also satisfactory. The average orientation of the ramp is 179.7/31.3W, and the standard deviation is 0.9°.
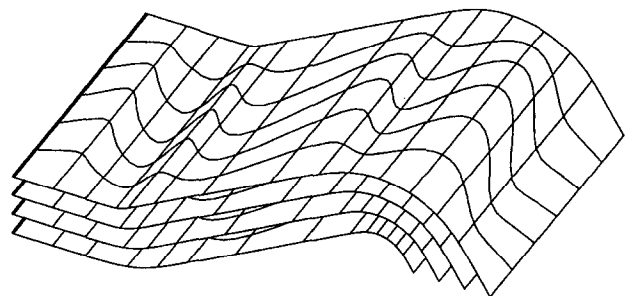
Table 1. For the theoretical examples of Figs 10, 12, 14, 15 and 18, and for the three least-squares criteria, this table shows the quality indices, I, computed after optimization and the weights, W, used in the overall objective function

	Horizontality		Bed-length		Volume	
	I_h	W_h	I_i	W_l	I_v	W_v
Fig. 10	4.7°	1.0	0.5%	1.0	0.5%	1.0
Fig. 12	0.5°	10.0	0.2%	1.0	1.3%	0.001
Fig. 14	0.1°	10.0	0.4%	1.0	1.5%	0.01
Fig. 15	4.6°	0.01	8%	1.0	0.5%	10.0
Fig. 18	0.6°	1.0	1.7%	0.1	0.6%	1.0

Fig. 11. A cylindrical thrust described by a crooked parameterization which explains the waves in the iso-u^2 contour lines. The fold *geometry* is identical to Fig. 10(a) (except a smaller thickness).
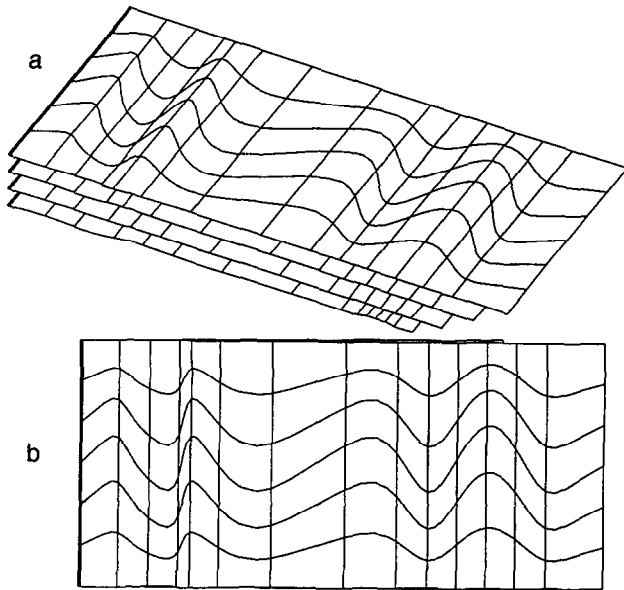
Fig. 12. Same model as Fig. 11 after unfolding. (a) Perspective view. (b) Top view. Owing to a geometric formulation, the result is insensitive to the idiosyncrasies of parameterization.
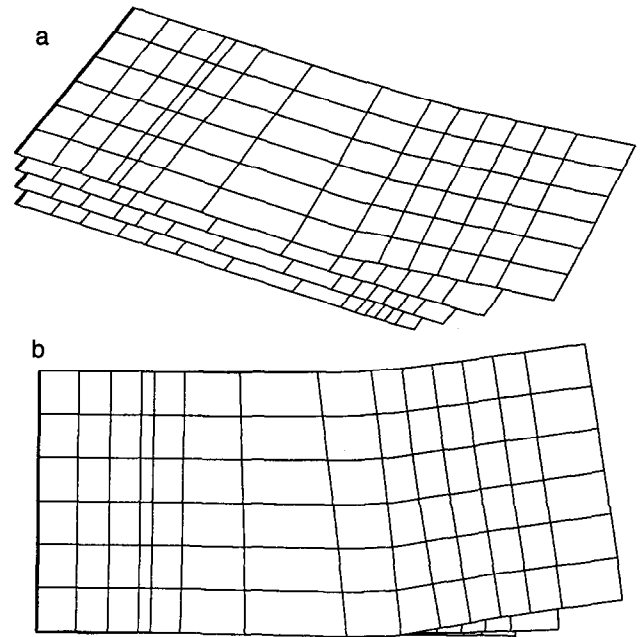

Fig. 14. Same model as in Fig. 13 after unfolding with priority given to horizontality. (a) Perspective view. (b) Top view.

A noncylindrical example

Folded foliations were exactly cylindrical in the previous examples, and a 3D approach was not necessary for them. Now we use a noncylindrical example to illustrate various possible compromises between conflicting hypotheses. The foliation in Fig. 13 shows a local warp. Therefore, horizontality and volume conservation cannot be exactly met together. Besides, since the folded foliation is no longer symmetrical, unfolding is expected to induce 3D effects.

First, if we give priority to the horizontality criterion ($w_h = 10$) as opposed to the volume conservation criterion ($w_v = 0.01$), the warp in the folded foliation, which attenuates from front to back, induces a boomerang like shape (Fig. 14). Quality indices are very satisfactory for horizontality (0.1°) and bed-length conservation (0.4%), but rather poor for volume conservation (15%).

If we give priority to volume conservation ($w_v = 10$) as opposed to horizontality ($w_h = 0.01$), we obtain the result shown in Fig. 15. The warp visible on the folded foliation spreads across the entire thickness of the unfolded foliation, which becomes horizontal on average. As a result, the upper leaf does not show rotation about the vertical axis (Fig. 14)
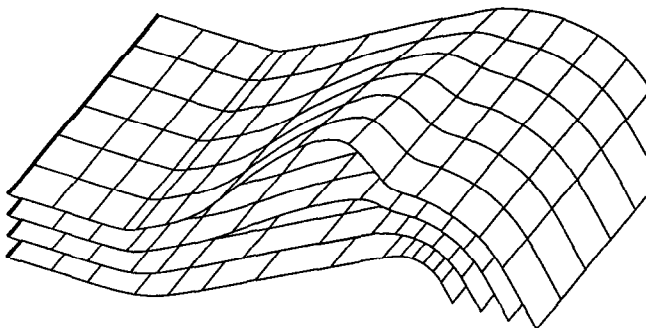

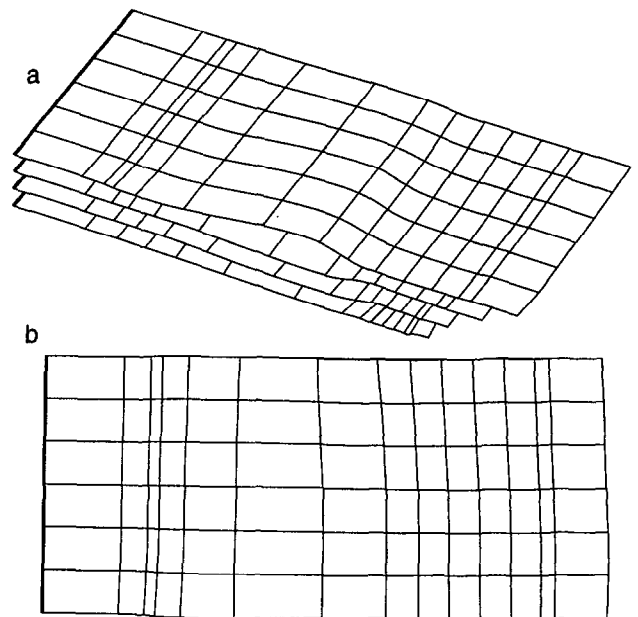Fig. 13. A folded noncylindrical and nonparallel foliation.

Fig. 15. Same model as in Fig. 13 after unfolding with priority given to volume conservation. (a) Perspective view. (b) Top view.

THE 'PAPERBACK' EXPERIMENT

The analog model

A folded paperback book was constructed with successive differently coloured sheets of paper (27 mm thick and 21 × 29.7 cm in width and length). This multi-surface paperback book model was pressed between rigid wooden molds and consolidated by foam injection. The model was then sawn along sixteen parallel cross-sections. These cross-sections were digitized, and five parallel folded surfaces were drawn. A schematic map view of the model is given in Fig. 1(b). For this example, the accuracy of the unfolding process given by the inverse method was compared with the results given by the UNFOLD finite element program (Gratier *et al.*, 1991). The folded surface is divided into rigid triangles, which are then laid flat and fitted by a least-squares method. For our example, the UNFOLD program fits the triangles with an uncertainty value of about 0.5%.

The numerical folded model

From the 16 digitized cross-sections, we selected the 13 that completely cross each foliation leaf from the binding to the opposite face. Next, we interactively constructed a set of 1296 B-spline parameters used to reconstruct these cross-sections satisfactorily. Figure 16 shows the agreement between digitized and computed cross-sections for 3 of them. Figure 17 shows a perspective view of the reconstructed folded model. This procedure fixes $\tilde{\Phi}$.

The results

Figure 18 shows the result of unfolding. We computed

Fig. 17. Perspective view of the folded model. By construction, rear and front faces correspond to cross-sections 1 and 13, hence they are vertical and orthogonal to the binding surface (left face). They do not correspond to original lateral faces.

50 orientation values on the face opposite the binding (Fig. 19). The dispersion is moderate (9°), and the average value is accurate (000.5/89.4W instead of 000/90). In our opinion, this result is satisfactory since many causes

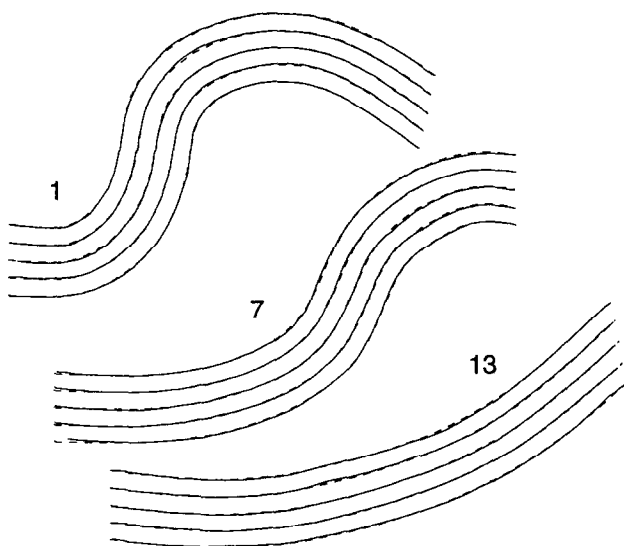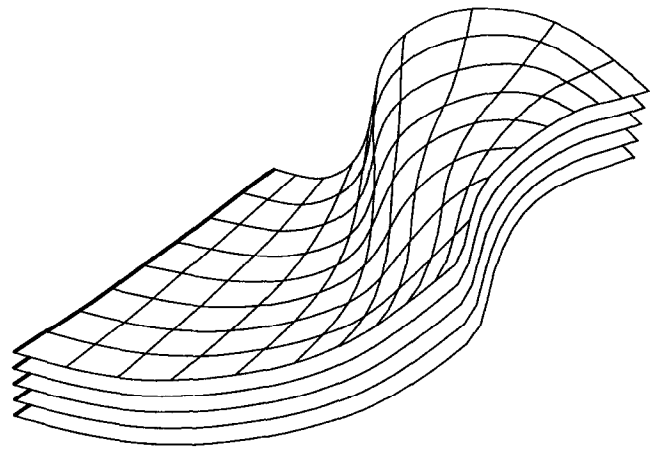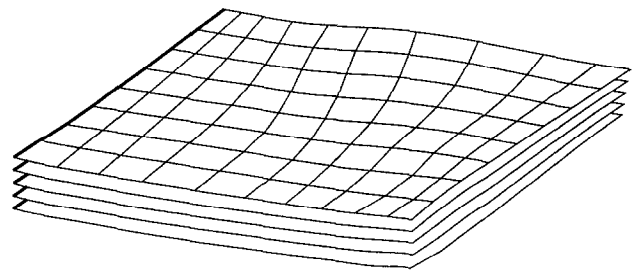Fig. 18. Model of Fig. 17, after unfolding.

Fig. 16. Digitized cross-sections 1, 7 and 13 (solid lines) and corresponding cross-sections computed from the set of B-spline parameters (dashed lines). Scale: 35% of the original.
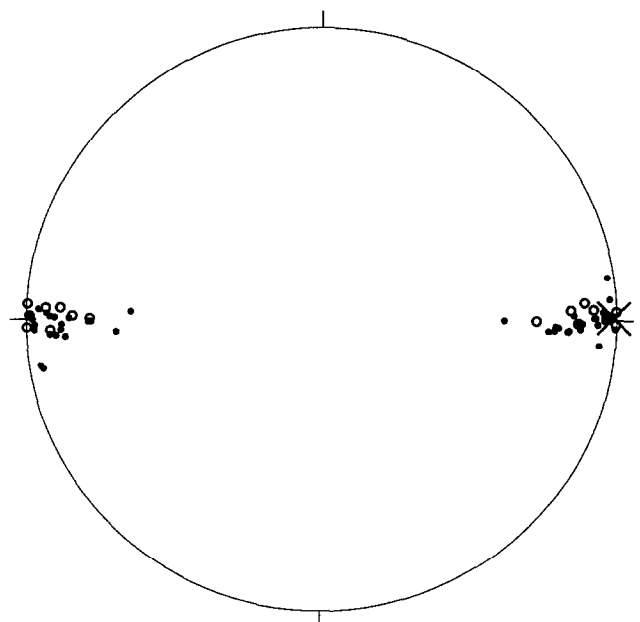

Fig. 19. In this stereographic chart (lower hemisphere projection), dots represent 50 orientations spread out on the face opposite the binding (the right face). The cross represents average value 000.5/89.4W (ideally 000/90). The standard deviation is 9°. Circles represent 17 orientations measured on the same face, obtained with the program UNFOLD.

contribute to this dispersion: the construction of the model, digitizing, B-spline parameter elaboration and numerical unfolding.

Seventeen orientations were estimated on the same face of the model obtained with UNFOLD (circles, on Fig. 19). Two successive points on the boundary of a same leaf define the strike, and a third point on the next leaf boundary gives the dip. Such measurements amplify possible length differences between successive surfaces: a difference of 1% in length (2.1 mm) corresponds to a 17° dip deviation from the vertical. This is the maximum dispersion observed with both methods. An uncertainty below 1% for bed-length conservation seems rather satisfactory for application to natural structures.

CONCLUSIONS

We advocate an inversion approach for multisurface restoration because it yields a compromise between conflicting assumptions. This method involves defining three least-squares objective functions, representing three assumptions — horizontality, bed-length conservation and local volume conservation — and in optimizing their weighted sum. This inversion method has been successfully tested on several theoretical examples. A cylindrically folded multisurface was unfolded without any problem. A nonparallel folded structure was also unfolded in order to test the effect of the weighting parameters. With emphasis on the local volume conservation against the horizontality of the restored structure, the unfolding of nonparallel structures is possible with thickness conservation. This is one of the main advantages of multisurface approaches, since single layer restoration methods cannot conserve volume for nonparallel layering. Currently, our own method renders surfaces horizontal on average. A future improvement could be to constrain one particular surface to be exactly horizontal, so as to restore the structure at the deposition time of that surface. Our inversion method was also successfully tested on an experimental analog example, consisting of a noncylindrical parallel folded paperback book. The accuracy of the multisurface inverse method is comparable to the accuracy of a single-layer finite element method (UNFOLD program). An advantage of the B-spline parametric representation of multisurface structures is that these surfaces are naturally smooth. However, modeling *chevron* folds is difficult because the parameterization degenerates. Weighted multicriteria optimization needs much computer time. Nevertheless, the key advantage of our restoration method is that it can reconcile conflicting assumptions.

Both folds and faults are common in nature. In such cases, since folded units are bounded by faults, the main problem with three-dimensional unfolding is the fitting of the restored blocks along the faults. Most of the time, fault geometry is less well known than folded layer geometry. Despite some recent improvements in interpolation tools for faults (inverse method integrating a

thread criterion, Thibaut *et al.*, 1996) the three-dimensional compatibility between folds and faults remains a target, especially integration of kinematic constraints between folding and faulting processes.

REFERENCES

Barr, D. (1985) 3D palinspastic restoration of normal faults in the Inner Moray Firth: implication for extensional basin development. *Earth and Planetary Science Letters* **75**, 191–203.

Bennis, C., Vézien, J. M. and Iglesias, G. (1991) Piecewise surface flattening for non-distorted texture mapping. *Computer Graphics* **25**, 237–246.

Cobbold, P. R. and Percevault, M.-N. (1983) Spatial integration of strains using finite elements. *Journal of Structural Geology* **5**, 299–306.

Dahlstrom, C. D. A. (1969) Balanced cross-sections. *Canadian Journal of Earth Science* **6**, 743–757.

Etchecopar, A. (1977) Plane kinematic model of progressive deformation in poly-cristalline aggregate. *Tectonophysics* **39**, 121–139.

Gibbs, A. (1983) Balanced cross-section construction from seismic sections in areas of extensional tectonics. *Journal of Structural Geology* **5**, 153–160.

Gratier, J. P., Guillier, B., Delorme, A. and Odonne, F. (1991) Restoration and balance of a folded and faulted surface by best-fitting of finite elements: principles and applications. *Journal of Structural Geology* **13**, 111–115.

Gratier, J.-P. and Guillier, B. (1993) Compatibility constraints on folded and faulted strata and calculations of total displacement using computational restoration (UNFOLD program). *Journal of Structural Geology* **15**, 391–402.

Kerr, H. G., Whim, N. and Brun, J. P. (1993) An automatic method for determining three-dimensional normal fault geometries. *Journal of Geophysical Research* **98**, 17837–17857.

Léger, M., Morvan, J. M. and Rakotoarisoa, H. (1995) Inversion of 3D structural geometry using geological least-squares criteria. *Geophysical Journal International* **121**, 63–81.

Lisle, R. J. (1992) Constant bed-length folding: three dimensional geometrical implications. *Journal of Structural Geology* **14**, 245–252.

McCoss, A. M. (1988) Restoration of transpression/transtension by generating the three-dimensional segmented helical loci of deformed lines across structure contour maps. *Journal of Structural Geology* **10**, 109–120.

Ramsay, J. G. (1967) *Folding and Fracturing of Rocks.* McGraw-Hill, New York.

Ramsay, J. G. (1969) The measurement of strain and displacement in orogenic belts. In *Time and Place in Orogeny*, eds P. E. Kent, G. E. Salter-Thwaite and A. M. Spencer, pp. 43–79. Special Publication of the Geological Society, London 3.

Ramsay, J. G. and Huber, M. I. (1987) *The Techniques of Modern Structural Geology, Volume 2: Folds and Fractures.* Academic Press, London.

Shaw, J. H., Hook, S. C. and Suppe, J. (1994) Structural trend analysis by axial surface mapping. *Bulletin of the American Association of Petroleum Geologists* **78**, 700–721.

Suppe, J. (1983) Geometry and kinematics of fault-bend folding. *American Journal of Science* **283**, 684–721.

Tarantola, A. (1987) *Inverse Problem Theory.* Elsevier, Amsterdam.

Thibaut, M. (1994) Géométrie des surfaces de faille et dépliage 3D (méthodes et applications). Ph.D. thesis, University of Grenoble. Éditions Technip, Paris.

Thibaut, M., Gratier, J.-P., Léger, M. and Morvan, J.-M. (1996) An inverse method for determining three-dimensional fault geometry with thread criterion: application to strike-slip and thrust faults (Western Alps and California). *Journal of Structural Geology* **18**, 1127–1138.

Woodward, N. B., Boyer, S. E. and Suppe, J. (1985) *An Outline of Balanced Cross-sections.* University of Tennessee Department of Geological Sciences Studies in Geology **11**.